IEEE Access
Multidisciplinary ⋮ Rapid Review ⋮ Open Access Journal

Received 14 December 2022, accepted 31 December 2022, date of publication 10 January 2023, date of current version 19 January 2023.

Digital Object Identifier 10.1109/ACCESS.2023.3235761

RESEARCH ARTICLE

Mutual Coupling Reduction in Dual-Band MIMO Antenna Using Parasitic Dollar-Shaped Structure for Modern Wireless Communication

CHOW-YEN-DESMOND SIM[1], (Senior Member, IEEE), VIGNESWARAN DHASARATHAN[2], (Member, IEEE), THIEN KHANH TRAN[2], (Member, IEEE), JAYSHRI KULKARNI[3], (Senior Member, IEEE), BRIAN A. GARNER[3], AND YANG LI[3], (Senior Member, IEEE)

[1]Electrical Engineering Department, Feng Chia University, Taichung 407102, Taiwan
[2]Chemical Engineering in Advance Materials and Renewable Energy Research Group, School of Engineering and Technology, Van Lang University, Ho Chi Minh City 700000, Vietnam
[3]School of Engineering and Computer Science, Baylor University, Waco, TX 76706, USA

Corresponding author: Jayshri Kulkarni (jayshri_kulkarni@baylor.edu)

This work was supported in part by the Ministry of Science and Technology (MOST), Taiwan, under Project MOST 111-2221-E-035-022.

ABSTRACT A dual-band Multiple Input Multiple Output (MIMO) antenna with low mutual coupling is analyzed and studied for Fifth Generation (5G) Sub-6 GHz and Wireless Fidelity (Wi-Fi) 6E frequency-band applications. Each of the identical monopole radiators consists of a rectangular patch, inverted-E, and asymmetrical T-shaped strip to generate 5G Sub-6 GHz and Wi-Fi 6E frequency bands. The deployment of the radiators horizontally with end-to-end separation of 5mm makes the antenna compact with an overall dimension of 45 × 30mm^2 (0.37λ×0.25λ for λ at the lower resonating frequency of 2.5GHz). The antenna achieves measured impedance bandwidths of 2.39-2.57 GHz and 3.82-6.95 GHz, respectively, at two resonating frequencies of 2.5 GHz and 4.5 GHz. A Parasitic Dollar Shaped Structure (PDSS) introduced between the two monopole radiators to suppress the surface waves of each monopole reduces the measured mutual coupling up to -15 dB throughout the operating band. Furthermore, the measured gain, radiation efficiency, Envelope Correlation Coefficient (ECC), and Diversity Gain (DG) values remain in good agreement with simulated values and are well within the minimum limit set by industry standards. These results affirm the applicability of the MIMO antenna for 5G and Wi-Fi 6E frequency bands.

INDEX TERMS Rectangular patch, PDSS, mutual coupling, inverted E-shaped, asymmetrical T-shaped, monopole radiators, sub-6 GHz, Wi-Fi 6E.

I. INTRODUCTION

Today's new generations of cellular and wireless Local Area Network (LAN) technologies, 5G and Wi-Fi 6E use common technical methodologies such as orthogonal frequency-division multiplexing (OFDM), and MIMO to provide high-end user experiences, power gigabit speed, and quicker response to users. Wi-Fi 6E uses an unlicensed frequency spectrum of 2.4-2.5 GHz and 5.15-7.125 GHz efficiently to achieve higher user densities with improved network efficiency. The 5G New Radio (5G NR) Sub-6 GHz requires a licensed spectrum of n77 (3.30-4.20 GHz), n78 (3.30-3.80 GHz), and n79 (4.40-5.00 GHz). While Wi-Fi 6E is easier to use and has become the dominant connectivity technology for homes and businesses, 5G offers the quality of service (QoS) for latency- and capacity-sensitive applications, including Industrial Internet of Things (IIoT) and robots. Therefore, building a MIMO antenna with a compact size and dual /multiband operations is desirable to allow both Wi-Fi 6E and 5G bands to be used independently and with a seamless transition in indoor networks. One particular challenge involved with the MIMO antenna design is the

The associate editor coordinating the review of this manuscript and approving it for publication was Raghvendra Kumar Chaudhary.

mutual coupling between closely deployed antenna elements which deteriorates the effectiveness of the MIMO antenna with respect to efficient utilization of available spectrum and high-speed data rate. Therefore, the MIMO antenna design with regulated mutual coupling within the current miniaturized printed antenna elements is critical for the advancement of MIMO antenna technology in the Wi-Fi 6E and 5G Sub-6 GHz bands.

In light of these challenges, several MIMO antennas aiming to reduce mutual coupling among closely-deployed antenna radiators for wireless applications are suggested in [1], [2], [3], [4], [5], [6], [7], [8], [9], [10], [11], [12], [13], [14], [15], [16], and [17]. The Ultra-wideband (UWB) antennas in [1] and [2] operating in the 4-12 GHz and 2.95-15.65 GHz bands, respectively, achieved high isolation using Quad G-shaped metamaterial and a parallel strip resonator. However, UWB technology is nearly obsolete today due to issues of co-existence and interference with other wireless technologies. To overcome this problem, several researchers have designed antennas for 5G Sub-6 GHz and WLAN applications. The antenna in [3] functions in the 5G Sub-6 GHz band and uses a slot in the ground plane to achieve good isolation. However, the antenna only achieved the isolation of -10 dB with 6-dB impedance bandwidth by using pin diodes (which increase power consumption and complexity) and occupied a very large space of $120 \times 60\text{mm}^2$. Two simpler antennas occupying less space ($30 \times 30\text{mm}^2$ and $40 \times 40\text{mm}^2$, respectively) are discussed in [4] and [5]. These antennas have very narrow bandwidth and operate in a single band only. In order to accommodate the multiband and wideband two-port MIMO, other antennas have been investigated in [6], [7], and [8]. The inverted-F antenna in [6] uses an inverted T-shaped slot to improve isolation and operates in the 3.3-3.65 GHz and 4.8-5.50 GHz bands. The CPW-fed antenna in [7] uses two identical trapezoidal radiating elements to achieve dual bands and a rectangular stub along with a defective ground to obtain a good isolation between the antenna radiators. The design in [8] uses a swastika slot in a rectangular patch to obtain dual bands, and a T-shaped strip to improve the isolation. Nevertheless, none of these antennas operate in both Sub-6 GHz and Wi-Fi 6E operating bands. The one exception is the MIMO antenna in [9], which operates in both the Sub-6 GHz and Wi-Fi 6E and achieves high isolation with a comb-shaped structure but has a disconnected ground that may not be suitable for diverse MIMO applications.

Nowadays, many researchers are oriented toward designing Dielectric Resonator Antennas (DRA) as these provide several advantages such as higher bandwidth, lower losses (due to the absence of metal), and improved gain and efficiency [10], [11], [12], [13], [14]. Researchers in [10] report an aperture-coupled, fed, two-port DR MIMO antenna built on a Roger's dielectric slab with impedance bandwidth of 4.70- 6.20 GHz and a mutual coupling of up to −15 dB operating in the WLAN 5 GHz band. Another two-port DR MIMO antenna mentioned in [11] operates in a single band with a 10-dB impedance between 5.65-6.55 GHz and a mutual coupling of up to −20 dB across the functioning bands. The DR antenna in [12] uses a ring-shaped DR and a defective ground structure to obtain the desired dual-band and uses polarization diversity to improve the isolation among the radiators. In [13], a two-port DRA MIMO antenna operates in the WLAN and Worldwide Interoperability for Microwave Access (WiMAX) bands with a dual-band of 3.30-3.80 GHz, and of 5.00-5.70 GHz, with mutual coupling better than −20 dB across the desired operating bands. In [14], two half-cylinder DRA's are placed next to each other without a gap to operate in dual bands, but each DRA operates in a separate band. However, a DRA is three-dimensional (3D) and thus occupies more physical space, which makes it less suitable for integration into next-generation wireless devices.

It can be seen that obtaining a dense MIMO antenna with minimum mutual coupling and accompanied by better diversity performance is still an important objective for research. The planar circularly polarized (CP) MIMO antennas are becoming a commonly used part of modern wireless devices, as these CP MIMO antennas minimize the problems of polarization mismatch and interference of the wireless signals. Planar CP MIMO antennas are investigated in [15], [16], and [17] for wireless applications. In [15], a simple modified square patch is used to generate CP waves at 5.6 GHz WLAN frequency with higher isolation of up to −37 dB. The compact antenna in [16] can also achieve CP radiation by embedding three oval slots on the right, left, and top concentric rings. This suggested CP technique produces CP waves in the 3.30-5.02 GHz band for 5G applications. The left-hand CP antenna in [17] uses a rectangular slot on a rectangular-shaped ring to operate in the 3.30-4.20 GHz frequency band with mutual coupling better than -15 dB across the operative band. However, none of these CP MIMO antennas operate in the Wi-Fi 6E bands.

In this paper, a compact two-antenna MIMO is designed on an economical FR-4 dielectric slab with a very small footprint of $45 \times 30\ \text{mm}^2$. The proposed dual-band MIMO antenna operates in the 5G Sub-6 GHz and Wi-Fi 6E bands with measured impedance bandwidths of 2.39-2.57 GHz and 3.82-6.95 GHz, respectively. The proposed antenna uses a novel Parasitic Dollar Shaped Structure (PDSS) which improves the isolation of the proposed MIMO antenna. Due to its compact size, dual-band operation in 5G Sub-6 GHz and Wi-Fi 6E bands, and reduced mutual coupling between the antenna radiators, the proposed MIMO antenna will be a good candidate for future next-generation wireless devices.

II. DESIGN STRUCTURE AND WORKING MECHANISM OF A SINGLE MONOPOLE RADIATOR

The layout and appearance of the single monopole radiator is illustrated in Figure 1.

Here, the main rectangular monopole is loaded with an inverted E-shaped structure at its left and an asymmetrical T-shaped strip at its right. To achieve better impedance matching of the CPW-feed technique, two identical ground planes

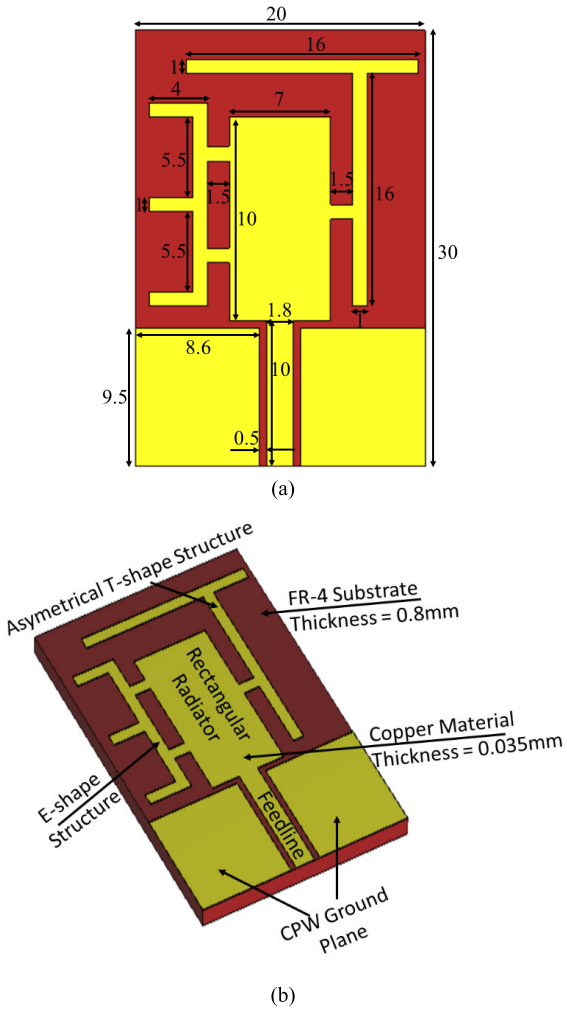

FIGURE 1. Layout of monopole radiator (a) Front View (b) Layered View.

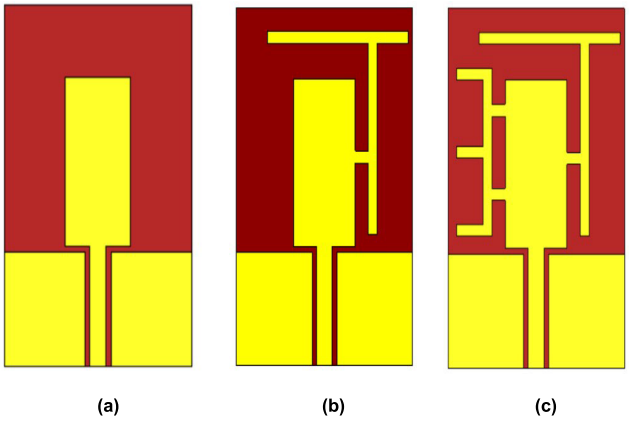

FIGURE 2. Step-wise development of the mechanism of the single monopole radiator (a) ANT@1 (b) ANT@2 (c) ANT@3.

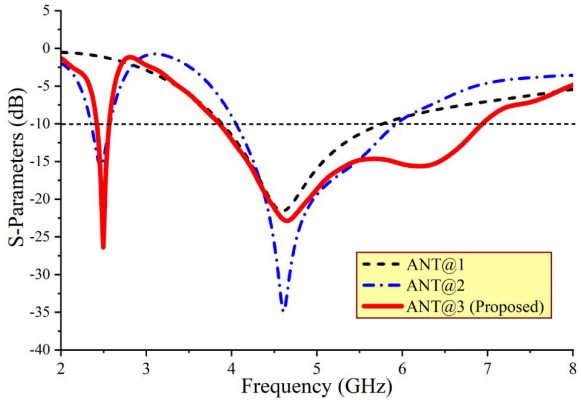

FIGURE 3. Corresponding S_{11} (dB) of step-wise design.

having an area of $8.6 \times 9.5\text{mm}^2$ each are positioned at the lower left and right corners of the substrate. A 50Ω microstrip transmission feeding line of size 10×1.8 mm^2 is embedded within the two ground planes with an air gap of 0.5mm on each side, as depicted in Figure 1. The overall planar size of this monopole radiator engraved on 0.8mm FR-4 substrate is 20×30 mm^3. To explore the working mechanism and excitation of the single monopole radiator within the two wide operational bandwidths of 2.40 to 2.55 GHz and 3.85 to 6.93 GHz, the remainder of this section describes the steps of antenna development and its corresponding reflection coefficient curve (S_{11}).

1) STEP 1: LOADING OF VERTICAL RECTANGULAR RADIATOR (ANT@1)

Initially, a vertical rectangular radiator (ANT@1) is introduced with symmetrical CPW-fed ground planes, as indicated in Figure 2a. The width and length of the vertical rectangular radiator were optimized using CST Microwave Studio®(MWS) to obtain the desired dimension of $14 \times 7\text{mm}^2$.

Figure 3 shows the associated S_{11} of ANT@1, indicating that ANT@1 induces a good resonant frequency at 4.5GHz with a wide bandwidth of 3.88-5.77 GHz. Thus, ANT@1 can meet the wideband demand for Sub-6 GHz 5G frequency band. The amalgamation of a vertical rectangular radiator, symmetrical ground planes, and microstrip feeding line cancels the reactive impedance by offering an equal amount of capacitive and inductive impedances at a resonating frequency of 4.5 GHz. Therefore, ANT@1 obtains good impedance matching for 3.88-5.77 GHz frequency bands.

2) STEP 2: DESIGN OF ASYMMETRICAL T-SHAPED STRIP (ANT@2)

As observed in Figure 3, the frequency band induced by ANT@1 alone is not sufficient to cover the lower and higher Wi-Fi 6E frequency band. Hence, in order to generate resonance at the lower frequency of 2.4 GHz as well as to enhance the bandwidth of the higher Wi-Fi 6E band without disturbing the impedance matching and feeding position of ANT@1, an asymmetrical T-shaped strip is deployed on the right side denoted as ANT@2 shown in Figure 2b. Here it can be observed that ANT@2 generates resonance at 2.5 GHz yielding a 10-dB impedance bandwidth between 2.40 and

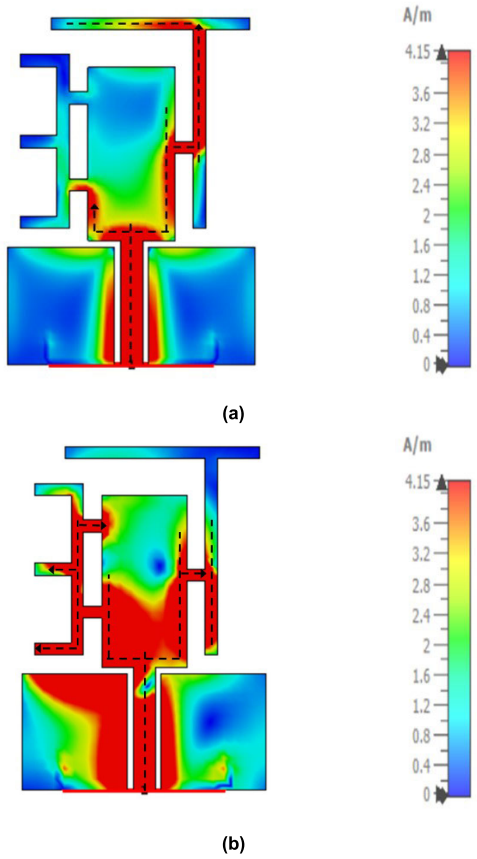

FIGURE 4. Surface current distribution of ANT@3 at (a) 2.5 GHz and (b) 4.5 GHz.

2.55 GHz, along with slight enhancement in the higher band of 4.11-6.01 GHz. (Figure 3). However, the ANT@2 still does not cover the higher Wi-Fi 6E band.

3) DEPLOYMENT OF AN INVERTED-E-SHAPED STRUCTURE (ANT@3)

In order to obtain the entire Wi-Fi 6E band, an inverted-E-shaped structure with equal-sized arms is deployed on the left side of ANT@2 (ANT@3, Figure 2c). Each of the three rectangular arms of the E-shaped structure has a size of 4×1 mm^2 (see Figure 1a), and, notably, the air gap between these arms acts as a capacitor to cancel the inductive reactance created by the E-shape. Furthermore, the entire inverted E-shaped structure increases the path for electrical current, thus aiding in enhancing the higher frequency bandwidth from (4.11-6.01 GHz) to the range of ANT@2 (3.85-6.93 GHz) along with better impedance matching at 2.5 GHz for ANT@3, as depicted in Figure 3. Therefore, the ANT@3 successfully functions in the lower frequency band of 2.40-2.55 GHz and higher frequency band of 3.85-6.93 GHz, thus fulfilling the desired frequency of Sub-6 GHz 5G and Wi-Fi 6E band.

To demonstrate the multiband and wideband characteristics of ANT@3, its respective surface current distribution is analyzed in Figure 4. From Figure 4a, it can be noticed that

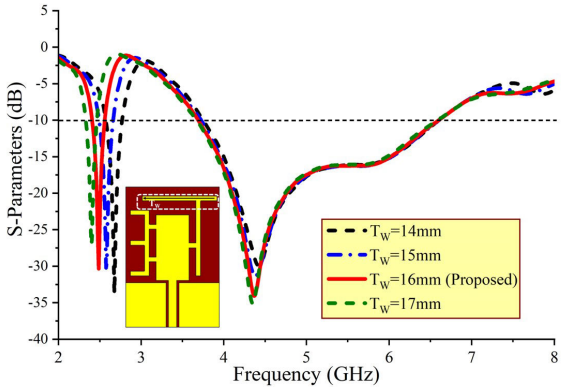

FIGURE 5. Simulated analysis of S_{11} versus frequency for varying the width T_W of asymmetrical T-shaped strip.

the maximum current is passing through the asymmetrical T-shaped strip (shown with black dotted lines), which helps to resonate at a lower 2.4GHz frequency band. Likewise, from Figure 4b, the longer current passing through the inverted E-shaped structure and the lower part of the asymmetrical T-shaped structure help in generating a resonance at 4.5GHz with a very wide bandwidth. Therefore, ANT@3 generates a dual band with impedance bandwidth of 6.06% (2.40-2.55 GHz) and 57.14% (3.85-6.93 GHz) at the resonant frequency of 2.5 GHz and 4.5 GHz, respectively, and will be applied for realizing the MIMO configuration for Sub-6 GHz 5G and Wi-Fi 6E applications.

III. PARAMETRIC ANALYSIS OF THE PROPOSED TWO-PORT MIMO ANTENNA

To characterize the proposed antenna in Sub-6 GHz 5G and Wi-Fi 6E bands, a parametric study of essential parameters like width (T_W) of asymmetrical T-shaped strip length (R_L) of the main monopole radiator, and length (G_L) of symmetrical ground planes are analyzed by keeping other dimensions unchanged.

A. A SIMULATED ANALYSIS OF VARIATION OF WIDTH T_W OF THE ASYMMETRICAL T-SHAPED STRIP

A simulated S_{11} of the proposed antenna versus frequency curve is plotted in Figure 5 for different values of T_w in the step increment of 1mm. From Figure 5, it can be noticed that as the width of T_w increases from 14 mm to 17 mm, the lower resonance of the 2.4 GHz band gets shifted toward the lower side of the spectrum. However, the variation of T_w does not affect the resonance of 4.5 GHz and the matching bandwidth of the Wi-Fi 6E band. To achieve the required bandwidth of lower 2.4 GHz band, the value of T_w as 16 mm is considered.

B. A SIMULATED ANALYSIS OF VARYING LENGTH R_L OF THE VERTICAL RECTANGULAR STUB

As observed from Figure 6, the impedance matching curves for the 2.4 GHz band remain unaffected for the variation R_L

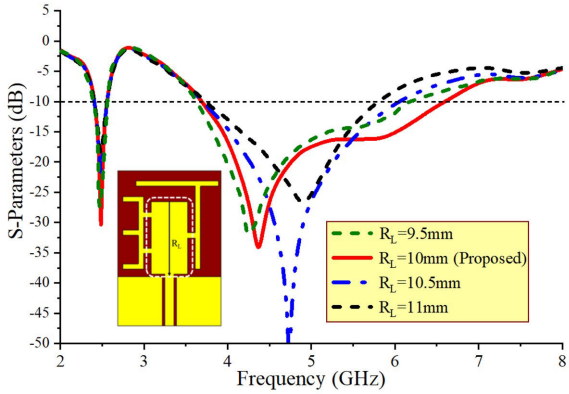

FIGURE 6. Simulated analysis of S_{11} versus frequency for varying the length R_L of vertical rectangular stub.

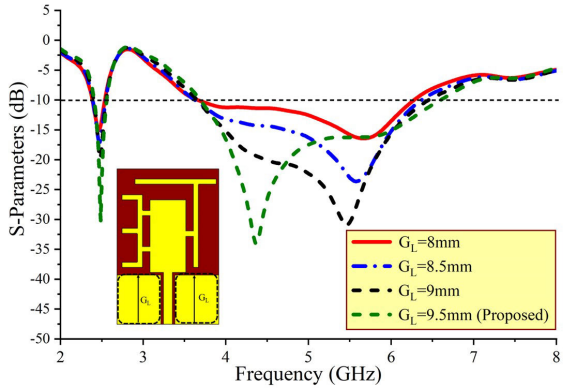

FIGURE 7. Simulated analysis of S_{11} versus frequency for varying the length G_L of CPW ground planes.

from 9.5 mm to 11 mm in the step increment of 0.5mm. The R_L of 9.5 mm affects the amplitude of S_{11} by reducing the required bandwidth. For R_L of 10.5 mm, the original resonance of 4.5 GHz is shifted towards the higher frequency of 4.8 GHz; however, this value of R_L fails to achieve the required band of Wi-Fi 6E. Further increment of R_L slightly shifts the resonance towards higher frequency and affects the value of S_{11} by decreasing the impedance bandwidth in the Wi-Fi 6E bandwidth. Therefore, R_L of 10 mm is considered as this gives the desired bandwidth of Wi-Fi 6E band with a good value of S_{11}.

C. SIMULATED ANALYSIS OF VARYING LENGTH G_L OF THE CPW GROUND PLANES

It can be seen from Figure 7 that the variation of G_L from 8 mm to 9.5 mm in a step increment of 0.5 mm has very less effect on the lower resonance of 2.4 GHz. However, it significantly affects the S_{11}, along with a slight deviation in 10-dB impedance bandwidth. It can be very well noted that decreasing G_L from 9.5 mm to 8 mm, slightly reduces the bandwidth at the same time, and decreases the S_{11} value of the Wi-Fi 6E band. Therefore, a G_L of 9.5 mm is considered in order to operate in the desired Wi-Fi 6E band.

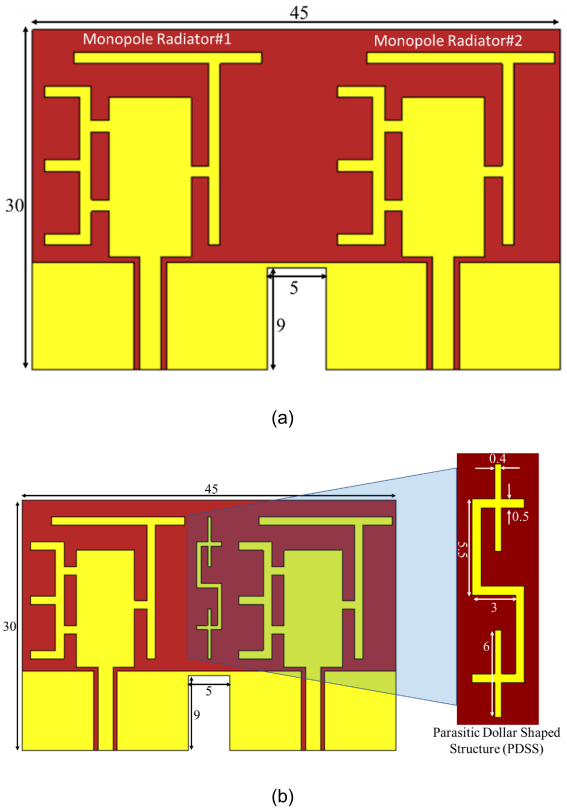

FIGURE 8. Layout and design of the proposed two-port MIMO, (a) without PDSS, and (b) with PDSS.

IV. LAYOUT AND ANALYSIS OF THE PROPOSED TWO-PORT MIMO ANTENNA

Figure 8 illustrates the layout and design of the proposed two-port MIMO antenna with and without deploying the isolating structure. As observed from Figure 8a, the two similar monopole radiators (ANT@3) are deployed horizontally at a distance of 0.04λ (where λ is the free space wavelength at 2.5 GHz). A compact PDSS is easily accommodated as a decoupling structure within this narrow space, as illustrated in Figure 8b. Furthermore, this narrow space also guarantees the monopole radiators will operate independently without affecting the MIMO diversity performance in a rich multipath scattering condition.

A. ANALYSIS OF TWO-PORT MIMO ANTENNA WITHOUT AND WITH PDSS LOADING

Figure 9(a) depicts the simulated S_{11} at port 1, S_{22} at port 2, and the mutual coupling (S_{12} and S_{21}) of the proposed two-port MIMO antenna without deploying the PDSS. Here, it can be noted that the S_{11} and S_{22} are similar, confirming good impedance matching in the operating bands. This configuration also exhibits wide 10-dB impedance bandwidths of 6.06% (2.40-2.55 GHz) and 57.14% (3.85-6.93 GHz). However, the mutual coupling level (S_{12} or S_{21}) of approximately −10 dB at around 4 GHz does not meet the industry and IEEE standards, which call for a lower than −15 dB

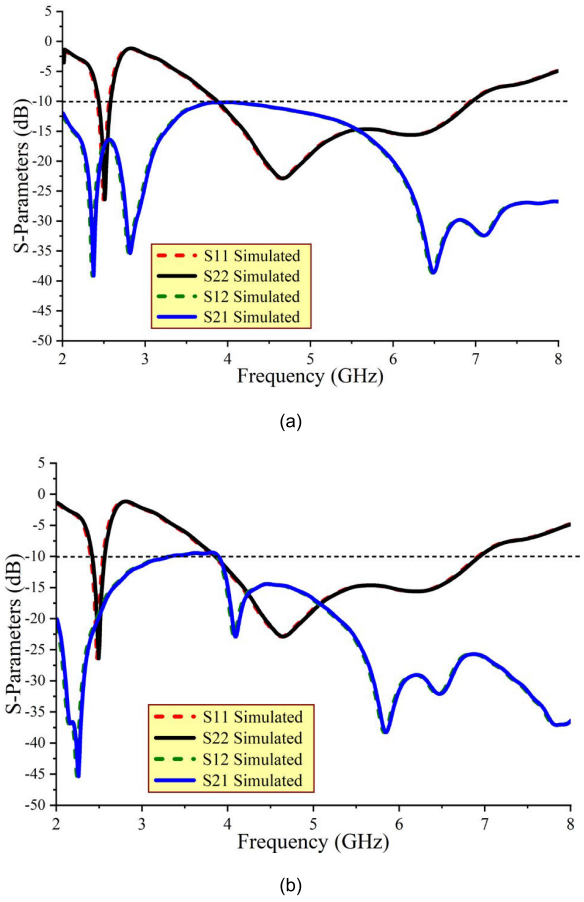

FIGURE 9. Simulated S-parameters (a) without the PDSS element (b) with PDSS element.

to communicate the antenna element independently without interfering with the adjacent antenna element.

Various techniques have been proposed to increase the isolation between two monopole radiators, including metamaterial [1], defected ground [3], EBG structure [4], comb-shaped structure [9], polarization diversity [12], and slotted ground structure [19]. For the antenna of this paper, a novel dollar-sign-shaped PDSS is employed as an isolating element between the monopole radiators (within the 0.04λ gap), as depicted in Figure 9b. The PDSS consists of two interlocking, opposite-facing C-shaped structures, each with a size of 5.5×3 mm^2. Further, a vertical rectangular strip of size 6×4 mm^2 is inserted on the lower arm of each C-shape in order to act as a stop band filter to block complete surface waves in the desired operating bands. The S-parameter curves in Figure 9b reveal that the introduction of the PDSS maintains the same impedance bandwidth (as observed from the S_{11}/S_{22} curves) of the monopole radiators. Notably, the PDSS significantly increases the isolation between the two monopole radiators, achieving a level of >15 dB (seen from S_{12}/S_{21} curves) and meeting industry standards.

Figure 10 shows the surface current (A/m) distribution without and with the PDSS structure at both the resonant frequency of 2.5 GHz and 4.5 GHz. Figure 10a reveals that at 2.5 GHz, when Monopole radiator#1 is active, but Monopole radiator#2 is terminated by 50 Ω load impedance, Monopole radiator#2 is highly coupled by the strong radiating field generated from Monopole radiator#1. In contrast, Figure 10b reveals that Monopole radiator#2 is shielded from the strong radiation field of Monopole radiator#1 due to the PDSS, which acts as a band stop filter to suppress the correlated signals (surface waves) coming from Monopole radiatort#1. The same phenomenon without PDSS (Figure 10c) and with PDSS (Figure 10d) at a 4.5 GHz resonant frequency is also shown and verified when Monopole radiator#2 is excited, while Monopole radiator#1 is terminated with a 50Ω load impedance.

B. PARAMETRIC ANALYSIS OF ISOLATING ELEMENT AND COMMON GROUND PLANE OF MIMO ANTENNA

To comprehend more about the performance of PDSS, a parametric study including the length (I_G) of the connected ground plane and width (I_D) of the vertical rectangular strip is carried out in the dual-band of operation of the proposed MIMO antenna. These critical parameters do not affect the desired resonances of 2.5 GHz and 4.5 GHz and achieve 10-dB impedance bandwidth. As noticed from Fig. 11, as the value of I_G increases from 7.5 mm to 9 mm in the step increment of 0.5 mm, the isolation level increases from 8 dB to 15 dB. The further increment of I_G fails to maintain the connectivity of ground planes of two identical monopole radiators, which is very essential in the practical implementation of the MIMO antenna. Therefore, an I_G of 9 mm is considered, as this helps to maintain the 15 dB isolation level throughout the dual-band operation.

Another analysis is carried out by increasing I_D from 0.2 mm to 0.8 mm, in the step increment of 0.2 mm, as illustrated in Fig. 12. It is noted that at the I_D of 0.2 mm, 15 dB isolation level is achieved in both desired operating bands; however, it was not considered for the final design of PDSS as the very thin size of 0.2 mm may create fabrication challenges. Furthermore, I_D of 0.6 mm and 0.8 mm shifts the isolation curve towards a higher frequency band. This results in a high isolation level of better than 15 dB at 4 GHz. Therefore, an I_D of 0.4 mm was considered for the final design of PDSS.

V. RESULTS AND DISCUSSION OF THE PROPOSED TWO-PORT MIMO ANTENNA

A prototype was fabricated to physically implement the proposed two-port MIMO antenna for Sub-6GHz 5G and Wi-Fi 6E wireless applications, as shown in Figure 13. The free space performances, including scattering and radiating, and MIMO diversity performances, including ECC and DG of the fabricated proposed prototype, were validated with simulated and experimental performances. When analyzing the two-port MIMO antenna, only one Monopole radiator was excited, whereas the other Monopole radiator was terminated with a 50Ω load impedance.

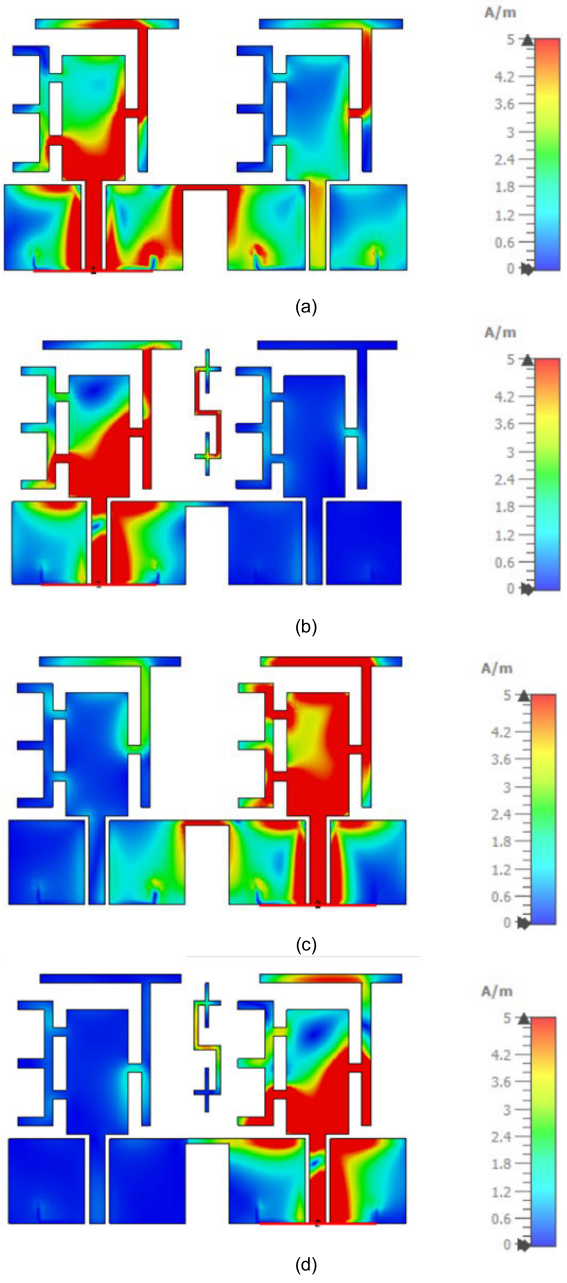

FIGURE 10. Surface Current (A/m) (a) without PDSS and monopole radiator#1 excited at 2.5GHz, (b) with PDSS and monopole radiator#1 excited at 2.5GHz, (c) without PDSS and monopole radiator#1 excited at 4.5GHz, and (d) with PDSS and monopole radiator#1 excited at 4.5GHz.

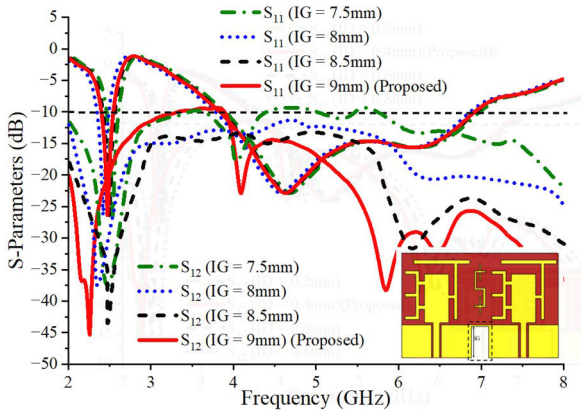

FIGURE 11. Simulation analysis of varying length (l_C) of the common ground plane on the isolation of proposed MIMO Antenna.

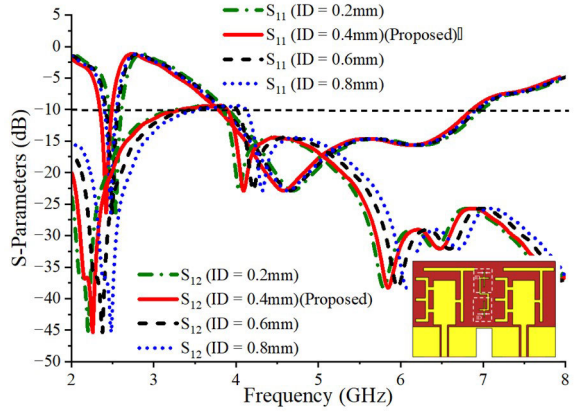

FIGURE 12. Simulation analysis of S_{12} vs frequency by varying the width (l_D) of the Isolating element.

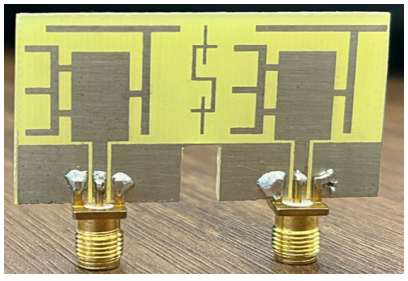

FIGURE 13. Fabricated prototype of the proposed two-antenna MIMO.

A. SIMULATED AND MEASURED S-PARAMETERS OF THE TWOPORT MIMO ANTENNA

As the S_{11} and mutual coupling S_{12} are analogous to S_{22} and S_{21}, respectively, Figure 14 only illustrates the simulated and measured S_{11} and S_{12} impedance bandwidth characteristics of the two-port MIMO antenna.

From Figure 14, it is important to note that both the simulated and measured results agree well with each other, with negligible variation in both operating bands. This small deviation may arise from minor fabricating errors or manufacturing tolerances. Nevertheless, Sub-6 GHz 5G and Wi-Fi 6E dual-band operation is clearly seen in Figure 14. The measured Sub-6 GHz 5G/lower Wi-Fi 6E and higher Wi-Fi 6E band operation exhibit wide 10-dB impedance bandwidths of 7.25% (2.39-2.57 GHz) and 58.12% (3.82-6.95 GHz), respectively, while the mutual coupling better than -15 dB was obtained in the desired bands.

B. SIMULATED AND MEASURED FAR-FIELD RADIATION PATTERNS OF TWO-PORT MIMO ANTENNA

Figure 16 depicts the schematic for far-field measurement inside an anechoic chamber. The radiation patterns of the

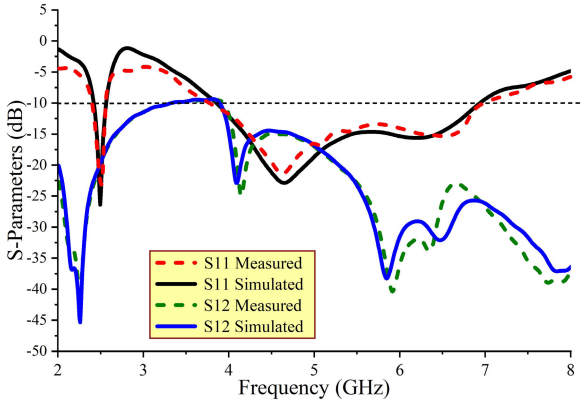

FIGURE 14. Simulated and measured S-parameters.

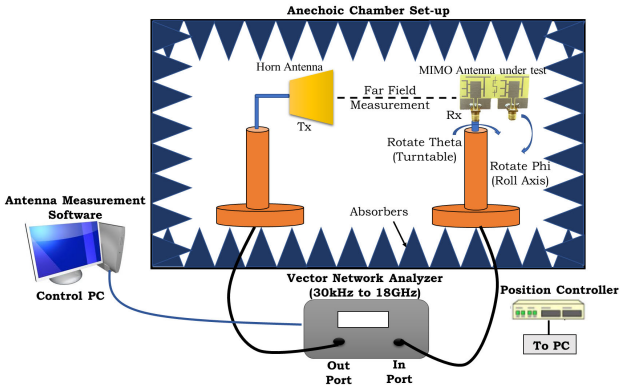

FIGURE 15. Schematic Diagram of anechoic chamber set-up for farfield measurements of antenna.

two-port MIMO antenna in the E-plane and H-plane are visualized in Figure 16.

Figures 16(a) and (b) reveal that the two monopole radiators in the E-plane exhibit approximately omnidirectional patterns and eight-shaped patterns for the co-polar and cross-polar radiation, respectively. Furthermore, it is important to observe that Monopole radiator#1's radiation patterns are exactly the mirror images of the ones shown in Monopole radiator#2. As for the H-plane equivalents, shown in Figures 16(c) and (d), across the two bands of operation, 2.5 GHz and 4.5 GHz, respectively, the two monopole radiators exhibit bi-directional patterns (co-polar) and omnidirectional patterns (cross-pol). These results demonstrate that the proposed two-port MIMO antenna offers reasonably good radiation far-field characteristics to meet the desired free space and MIMO diversity performances in rich multipath conditions.

C. SIMULATED AND MEASURED REALIZED GAIN AND RADIATION EFFICIENCY

Figure 17 shows the gain and efficiency plots of the two-port MIMO Antenna.

As the two monopole radiators are similar in structure and performance, only the characteristics of monopole radiator#1 are shown. The maximum simulated gain is observed to be

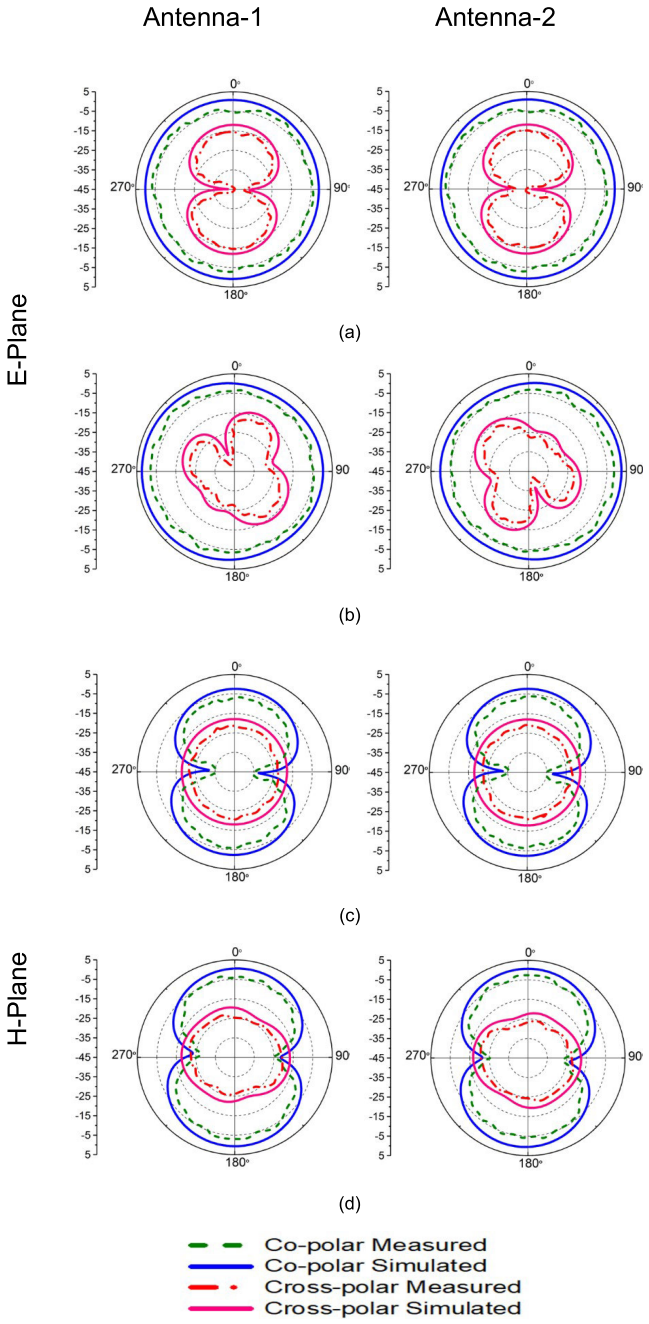

FIGURE 16. Radiation patterns of Monopole radiator#1 and Monopole radiator#2, at (a) 2.5 GHz, E-plane, (b) 4.5 GHz, E-plane, (c) 2.5 GHz, H-plane, and (d) 4.5 GHz, H-plane.

2.65 dBi, whereas the measured gain is 2.60 dBi. The peak simulated efficiency is observed to be 75%, while the measured efficiency is around 70%. Thus, the two-port MIMO antenna exhibits good gain and radiation efficiency.

VI. DIVERSITY PERFORMANCE ANALYSIS

To confirm the efficacy of the two-port MIMO antenna, the diversity assessment (ECC and DG, for example) are essential and thus was verified through both simulation and measurement.

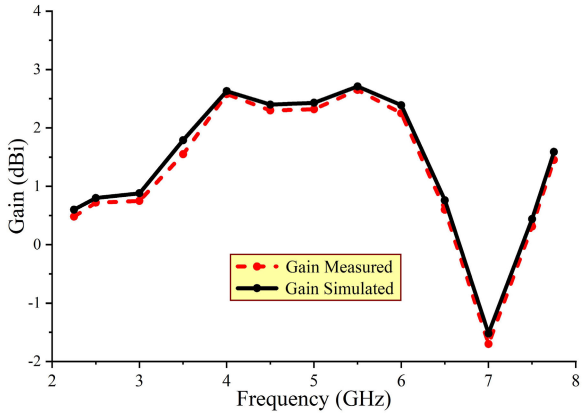

(a)

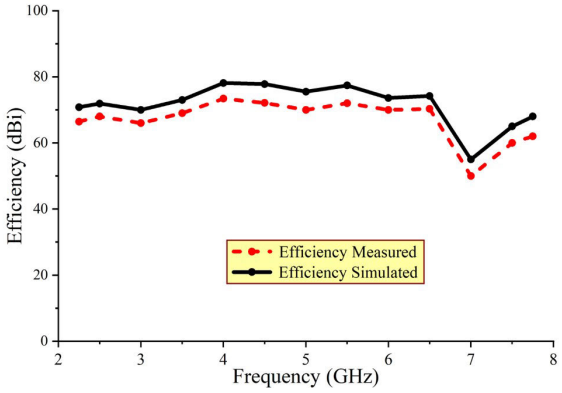

(b)

FIGURE 17. Gain (a) and Efficiency (b).

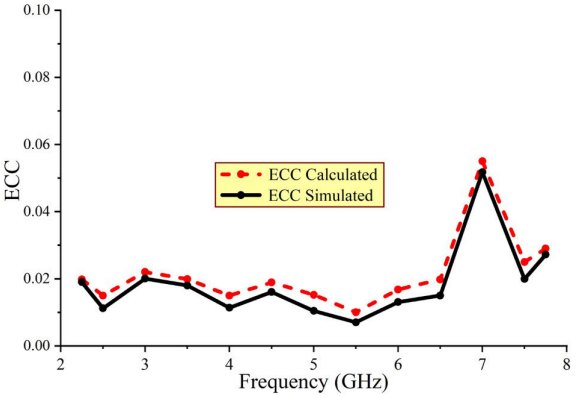

FIGURE 18. Calculated and simulated ECC.

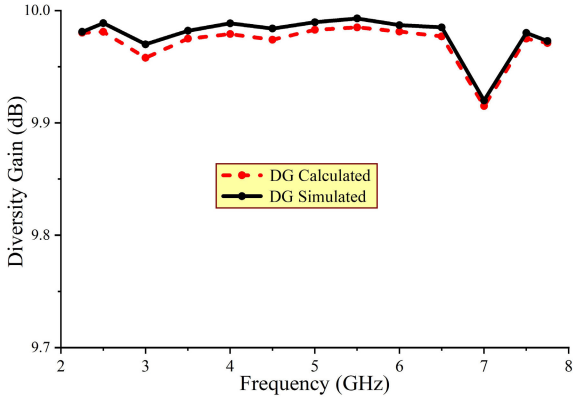

FIGURE 19. Calculated and simulated DG.

A. ENVELOPE CORRELATION COEFFICIENT (ECC)

The ECC was investigated to determine how independently the monopole radiators can radiate throughout the operating band. Ideally, the ECC value should be zero, which shows that monopole radiators do not interfere with each other despite close deployment and that each radiates independently by generating uncorrelated signals. However, in a real scattering situation, the ECC value is not zero. The ECC value of the two-port MIMO antenna is determined by the far-field patterns using Equations (1) [18].

$$\rho_e = \frac{\left| \iint_{4\pi} \left[F_1(\theta, \emptyset) * \overrightarrow{F_2}(\theta, \varnothing) \right] d\Omega \right|}{\iint_{4\pi} \left| \overrightarrow{F_1}(\theta, \emptyset) \right|^2 d\Omega \iint_{4\pi} \left| \overrightarrow{F_2}(\theta, \varnothing) \right|^2 d\Omega} \quad (1)$$

where F_1 (θ, ϕ) is the three-dimensional (3D) field pattern of the antenna when the i^{th} port is excited, and Ω is the solid angle.

Figure 18 depicts the ECC graph for the desired frequency ranges. The ECC of the two-port MIMO antenna obtained from equations (1) remain well below 0.02 in the complete operating band, which confirms that this MIMO antenna operates close to the ideal MIMO diversity performance criteria.

B. DIVERSITY GAIN (DG) dB

The DG parameter is used to calculate the increment in the signal-to-noise ratio (SNR) magnitude of each signal path because of the fading signals of the spatial diversity technique. Ideally, the DG is equal to 10 dB. Calculation of its value is obtained using Equation (2).

$$DG = 10\sqrt{1 - |\rho_e|} \quad (2)$$

Figure 19 illustrates the DG of the two-port MIMO antenna. The calculated and simulated DG results obtained from far-field radiation patterns are very near the ideal of 10 dB. This result indicates that the two monopole radiators are strongly mutually uncoupled and thus are suitable for MIMO applications.

VII. PERFORMANCE STUDY OF THE TWO-PORT MIMO ANTENNA

Performance comparison of the two-antenna MIMO is conducted with respect to the existing two-antenna MIMO types, including operating bands, size, type of decoupling structure, gain, efficiency, ECC, and DG (Table 1). Table 1 shows that the two-antenna MIMO exhibits sufficiently wide bandwidth and dual-band operation with smaller design footprints and acceptable ECC and DG values.

TABLE 1. Study of two-antenna MIMO.

Ref.	Area (mm2)	Operating Bands (GHz)	Band	Decoupling Structure	Isolation (dB)	Substrate	Gain (dBi)	Efficiency (%)	ECC	DG
5	1600	3.4 – 3.6	Single	Not Used	35	FR-4	2.4	81	0.01	-
6	792	3.3 – 3.65 4.8 – 5.5	Dual	Inverted T-shaped slot	18	FR-4	3.84	92.2	0.002	9.9
7	2500	2.25 – 3.15 4.89 – 5.95	Dual	Rectangular Stub	15	FR-4	5.59	77.8	0.01	9.8
8	1380	1.85 – 3.63 5.07 – 7.96	Dual	T-shaped strip	16	FR-4	1.14	72	0.003	9.99
9	1504	3.30 – 7.70	Single	Comb-shaped structure	18	FR-4	3	78	0.04	9.98
10	3200	4.70 – 6.20	Single	Not Used	15	Roger RT Duroid	2	87	0.2	9.9
12	2450	2.30 – 2.90 3.40 – 4.00	Dual	Defective Ground Structure	20	FR-4	2	90	0.2	9.80
13	3034	3.30 – 3.80 5.00 – 5.70	Dual	Polarization Diversity	15	FR-4	6	85	0.01	9.99
14	6400	5.71 – 8.20	Single	Not Used	20	FR-4	3.8	70	0.05	9.95
15	1125	5.23 – 6.42	Single	Ground Slot	17	FR-4	6	75	0.001	9.99
16	500	3.12 – 5.00	Single	Not Used	18	FR-4	2.5	70	0.01	-
17	1110	3.30 – 4.20	Single	Not Used	15	FR-4	1	95	0.15	9.92
Prop.	1350	2.40-2.57 3.85-6.96	Dual	Dollar-shaped Strip	15	FR-4	2.65	70	0.02	9.98

More specifically, from Table 1, the following features of the two-antenna MIMO are identified:

1. It has the smallest designed footprint (area) compared to [5, 7, 8, 9, 10, 12, 13, and 14].
2. Unlike [5, 9, 10, 14, 15, 16, and 17], it functions in a dual-band.
3. Higher gain than [5, 8, 10, 12, and 17].
4. Unlike [10, 12, and 17], it has greater ECC and DG.
5. Its decoupling structure is very compact and simple in design, giving high isolation of >15 dB compared to other designs researched in the literature.

VIII. CONCLUSION

A two-port MIMO antenna exhibiting the bandwidth requirements of Sub-6 GHz 5G and Wi-Fi 6E band has been successfully designed, studied, and analyzed. The two-port MIMO antenna validates dual-band operation with wide 10-dB impedance bandwidths of 7.25% (2.39-2.57 GHz) and 58.12% (3.82-6.95 GHz), along with a peak gain of 2.65 dBi and efficiency of 70%. Deployment of a dollar-sign-shaped PDSS as a decoupling structure between the two closely spaced monopole radiators of the MIMO antenna produces a desirable mutual coupling better than -15 dB. Assessment metrics such as ECC (< 0.02) and DG (> 9.98 dB) are found to be well within the acceptable practical values. Therefore, because of its good free-space characteristics, better diversity assessment, and small design footprint, the two-port MIMO antenna can be easily integrated inside modern devices functioning in the Sub-6 GHz 5G and Wi-Fi 6E bands. In addition, it is well suited to form large-number antenna arrays for better wireless communication transmission and reception signal quality and for facilitating seamless internet connectivity.

REFERENCES

[1] F. Urimubenshi, D. B. O. Konditi, J. D. D. Iyakaremye, P. M. Mpele, and A. Munyaneza, "A novel approach for low mutual coupling and ultra-compact two port MIMO antenna development for UWB wireless application," *Heliyon*, vol. 8, no. 3, Mar. 2022, Art. no. e09057.

[2] T. Addepalli and V. R. Anitha, "Compact two-port MIMO antenna with high isolation using parasitic reflectors for UWB, X and Ku band applications," *Prog. Electromagn. Res. C*, vol. 102, pp. 63–77, 2020.

[3] S. Padmanathan, A. A. Al-Hadi, A. M. Elshirkasi, S. S. Al-Bawri, M. T. Islam, T. Sabapathy, M. Jusoh, P. Akkaraekthalin, and P. J. Soh, "Compact multiband reconfigurable MIMO antenna for Sub- 6GHz 5G mobile terminal," *IEEE Access*, vol. 10, pp. 60241–60252, 2022, doi: 10.1109/ACCESS.2022.3180048.

[4] P. Ranjan, M. Patil, S. Chand, A. Ranjan, S. Singh, and A. Sharma, "Investigation on dual-port printed MIMO antenna with reduced RCS for C-band radar application," *Int. J. RF Microw. Comput.-Aided Eng.*, vol. 30, no. 3, Mar. 2020.

[5] M. Anbarasu and J. Nithiyanantham, "Performance analysis of highly efficient two-port MIMO antenna for 5G wearable applications," *IETE J. Res.*, pp. 1–10, May 2021, doi: 10.1080/03772063.2021.1926345.

[6] A. Chatterjee, M. Midya, L. P. Mishra, and M. Mitra, "Dual-element multiple-input-multiple-output system for sub-6 GHz (5G) and WLAN applications with enhanced isolation," *Prog. Electromagn. Res. M*, vol. 103, pp. 197–207, 2021.

[7] Y. Dou, Z. Chen, J. Bai, Q. Cai, and G. Liu, "Two-port CPW-fed dual-band MIMO antenna for IEEE 802.11 a/b/g applications," *Int. J. Antennas Propag.*, vol. 2021, pp. 1–8, Jun. 2021.

[8] R. N. Tiwari, P. Singh, S. Pandey, R. Anand, D. K. Singh, and B. K. Kanaujia, "Swastika shaped slot embedded two port dual frequency band MIMO antenna for wireless applications," *Anal. Integr. Circuits Signal Process.*, vol. 109, no. 1, pp. 103–113, Oct. 2021, doi: 10.1007/s10470-021-01923-x.

[9] J. Kulkarni, A. Desai, and C. Sim, "Two port CPW-fed MIMO antenna with wide bandwidth and high isolation for future wireless applications," *Int. J. RF Microw. Comput.-Aided Eng.*, vol. 31, no. 8, Aug. 2021, Art. no. e22700.

[10] S. Singhwal, B. Kanaujia, A. Singh, and J. Kishor, "Dual-port MIMO dielectric resonator antenna for WLAN applications," *Int. J. RF Microw. Comput.-Aided Eng.*, vol. 30, Apr. 2020, Art. no. e22108.

[11] M. Mishra, S. Chaudhuri, R. S. Kshetrimayum, A. Alphones, and K. P. Esselle, "Space efficient meta-grid lines for mutual coupling reduction in two-port planar monopole and DRA array," *IEEE Access*, vol. 10, pp. 49829–49838, 2022, doi: 10.1109/ACCESS.2022.3146941.

[12] G. Bharti, D. Kumar, A. K. Gautam, and A. Sharma, "Two-port ring-shaped dielectric resonator-based diversity radiator with dual-band and dual-polarized features," *Microw. Opt. Technol. Lett.*, vol. 62, no. 2, pp. 581–588, Feb. 2020, doi: 10.1002/mop.32053.
[13] T. Kumari, G. Das, R. K. Gangwar, and K. K. Suman, "Dielectric resonator based two-port dual band antenna for MIMO applications," *Int. J. RF Microw. Comput.-Aided Eng.*, vol. 29, Dec. 2019, Art. no. e21985.
[14] G. Varshney, R. Singh, V. S. Pandey, and R. S. Yaduvanshi, "Circularly polarized two-port MIMO dielectric resonator antenna," *Prog. Electromagn. Res. M*, vol. 91, pp. 19–28, 2020.
[15] I. Khan, Q. Wu, I. Ullah, S. U. Rahman, H. Ullah, and K. Zhang, "Designed circularly polarized two-port microstrip MIMO antenna for WLAN applications," *Appl. Sci.*, vol. 12, no. 3, p. 1068, Jan. 2022, doi: 10.3390/app12031068.
[16] J. Kulkarni, C.-Y.-D. Sim, R. K. Gangwar, and J. Anguera, "Broadband and compact circularly polarized MIMO antenna with concentric rings and oval slots for 5G application," *IEEE Access*, vol. 10, pp. 29925–29936, 2022, doi: 10.1109/ACCESS.2022.3157914.
[17] A. K. Dwivedi, A. Sharma, A. K. Pandey, and V. Singh, "Two port circularly polarized MIMO antenna design and investigation for 5G communication systems," *Wireless Pers. Commun.*, vol. 120, no. 3, pp. 2085–2099, Oct. 2021, doi: 10.1007/s11277-021-08461-9.
[18] A. G. Alharbi, J. Kulkarni, A. Desai, C.-Y.-D. Sim, and A. Poddar, "A multi-slot two-antenna MIMO with high isolation for sub-6 GHz 5G/IEEE802.11ac/ax/C-band/X-band wireless and satellite applications," *Electronics*, vol. 11, no. 3, p. 473, Feb. 2022, doi: 10.3390/electronics11030473.
[19] S. Nandi and A. Mohan, "A compact dual-band MIMO slot antenna for WLAN applications," *IEEE Antennas Wireless Propag. Lett.*, vol. 16, pp. 2457–2460, 2017, doi: 10.1109/LAWP.2017.2723927.

CHOW-YEN-DESMOND SIM (Senior Member, IEEE) was born in Singapore, in 1971. He received the B.Sc. degree from the Engineering Department, University of Leicester, U.K., in 1998, and the Ph.D. degree from the Radio System Group, Engineering Department, University of Leicester, in 2003. From 2003 to 2007, he was an Assistant Professor with the Department of Computer and Communication Engineering, Chienkuo Technology University, Changhua, Taiwan. In 2007, he joined the Department of Electrical Engineering, Feng Chia University (FCU), Taichung, Taiwan, as an Associate Professor, where he became a Full Professor, in 2012, and a Distinguish Professor, in 2017. He was an Executive Officer of Master's Program with the College of Information and Electrical Engineering (Industrial Research and Development) and the Director of the Intelligent IoT Industrial Ph.D. Program, from August 2015 to July 2018. He co-founded the Antennas and Microwave Circuits Innovation Research Center, Feng Chia University, and worked as the Director, from 2016 to 2019. Since October 2016, he has been serving as the Technical Consultant with the Securitag Assembly Group (SAG), which is one of the largest RFID tag manufacturers in Taiwan. He has been working as the Consultant with Avary (the largest PCB manufacturer in mainland China), since August 2018. He worked as the Head of the Department of Electrical Engineering, Feng Chia University, from August 2018 to July 2021. He has authored or coauthored over 190 SCI papers. His current research interests include antenna design, VHF/UHF tropospheric propagation, and RFID applications. He is a fellow of the Institute of Engineering and Technology (FIET), a Senior Member of the IEEE Antennas and Propagation Society, and a Life Member of IAET. He has served as a TPC member for many international conferences and has also served as the TPC Sub-Committee Chair (Antenna) for the ISAP 2014 and PIERS 2017/2019. He was a recipient of the IEEE Antennas and Propagation Society Outstanding Reviewer Award (IEEE TRANSACTIONS ON ANTENNAS AND PROPAGATION) for eight consecutive years, from 2014 to 2021. He has also received the Outstanding Associate Editor Award from the IEEE ANTENNAS WIRELESS AND PROPAGATION LETTERS, in July 2018. He has also served as the TPC Chair for the APCAP 2016 and iWEM 2019/2020, and the Track Chair for ICCC 2022. He was the General Co-Chair of ISAP 2021. He has served as the Chapter Chair for the IEEE AP-Society, Taipei Chapter, from January 2016 to December 2017, and the Founding Chapter Chair for the IEEE Council of RFID, Taipei Chapter, from October 2017 to December 2020. He has served as an Associate Editor for IEEE ACCESS, from August 2016 to January 2021. He is currently serving as an Associate Editor for IEEE ANTENNAS AND WIRELESS PROPAGATION LETTERS, IEEE JOURNAL OF RADIO FREQUENCY IDENTIFICATION, and *International Journal of RF and Microwave Computer-Aided Engineering*. He was invited as the Workshop/Tutorial Speaker in APEMC 2015, iAIM 2017, InCAP 2018, and APMC 2022, and an Invited Speaker of TDAT 2015, iWAT 2018, APCAP 2018, ISAP 2019, InCAP 2019, ISRAST 2020, ISAP 2020, NEAST 2020, URSI GASS 2021, iWEM 2021, WAMS 2022, and APCAP 2022. He was a Keynote Speaker of IEEE SOLI 2018. He has served as the Advisory Committee for InCAP 2018/2019 and ICoICCS 2021.

VIGNESWARAN DHASARATHAN (Member, IEEE) received the Ph.D. degree in information and communication engineering.

He is currently working with space division multiplexing applications for avoiding the cross-talk effects of dense network optical systems. In addition, he is also working in the field of photonics 2D materials, photonics sensing, nonlinear photonics, UWB antenna, and flexible antenna. He also moves his career as a selection grade of an Assistant Professor at the KPR Institute of Engineering and Technology. He is also working as a Visiting Scientist with the University of Hradec Králové, Czechia; Ton Duc Thang University, Vietnam; and Van Lang University, Vietnam. He has published around 100 articles in well-reputed journals, including IEEE, Nature, Springer, Wiley, SPIE, World Scientific Publisher, Taylor & Francis, IET, and OSA. His research interests include optical communication, photonic networks, and wireless optical communication in the higher end of the 5G networks.

Dr. Dhasarathan is also in one of the reputed editor panel members and serves as an Associate Editor for the *Wireless Networks* (Springer), *Optical and Quantum Electronics* (Springer), *Network Modeling, and Bioinformatics* (Springer), and *BMC Medical Imaging* (Springer). As a reviewer, he has reviewed more than 300 articles from various journals, including IEEE, Nature, and OSA. He has been declared as fastest and reviewer appreciation from Elsevier and Springer. His name has been listed in top 2% of scientist renowned by Stanford University, during 2021–2022. More information can be found at: https://scholar.google.co.in/citations?user=8_SSgkYAAAAJ&hl=en

THIEN KHANH TRAN (Member, IEEE) is currently a Lecturer/Researcher with the School of Engineering and Technology (VLSET), Van Lang University (VLU), Ho Chi Minh City, Vietnam, with a role of the Head of the Chemical Engineering in Advanced Materials and Renewable Energy Research Group (CME). In addition, he is also a member of the Institute for Circular Economy Development (ICED), Vietnam National University Ho Chi Minh City (VNU-HCM), with the role of the Head of the Circular Economy Development in Energy Research Unit. He spent seven years studying the art of renewable energy and chemical engineering in Taiwan (Long Hua University, Taipei, and Feng Chia University, Taichung City), where he found his unyielding interest in the major of hydrogen energy and material sciences. After graduate from the doctoral program with Feng Chia University, he went back to Vietnam to work at Ton Duc Thang University (TDTU) for four years before switch to VLU and a cooperation position with Vietnam National University (VNU). He has participated in many national and international cooperations, activities, and projects from universities to companies in recent years, providing his skills and knowledge in both training programs, technical content, and raising awareness activities. Not only that, he showed very good publication ability with good scientific reports, publications, and book chapters in reliable and renowned journals, since 2017.

JAYSHRI KULKARNI (Senior Member, IEEE) received the B.E. degree in electronics and tele-communication engineering from Shivaji University, Maharashtra, India, in 2005, the M.E. degree in microwave engineering from the PICT College, Pune, Maharashtra, in 2011, and the Ph.D. degree in electronics and communication engineering from Anna University, Chennai, India, in 2020.

From 2006 to 2009, she was a Lecturer with the Genba Sopanrao Moze College of Engineering, Pune. From 2010 to 2022, she was an Assistant Professor with the Electronics and Telecommunication Engineering Department, Vishwakarma Institute of Information Technology, Pune. She is currently working as a Postdoctoral Research Associate with Baylor University, Waco, TX, USA. She has authored more than ten books and more than 50 research papers in reputed journals and conferences. Her research interests include antennas, microwave engineering, wireless communications, and wireless sensor networks.

Dr. Kulkarni received several awards, including the Desmond Sim Award for Best Antenna Design Paper at IEEE InCAP 2019, India, the Outstanding Oral Presentation Award at ICRAMET-2020 Indonesia, and the Best Paper of the Session Award at IEEE ESCI-2021, Pune. She was one of the recipient of the reputed Mojgan Daneshmand Grant awarded by IEEE Antennas and Propagation Society (AP-S)-2022.

BRIAN A. GARNER received the B.S., M.S., and Ph.D. degrees in mechanical engineering from The University of Texas at Austin, in 1989, 1992, and 1998, respectively. During his Ph.D. pursuit and until 2001, he developed computer modeling software and served in technical roles for several private companies in Austin. He returned to The University of Texas at Austin, from 2001 to 2002, where he worked as a Faculty Lecturer with the Mechanical Engineering Department. He is currently an Associate Professor of mechanical engineering with Baylor University, where he has been working, since 2002. He is also an Inventor of MiraColt, a powered therapeutic mechanical device that simulates the motion experienced when riding on a horse, and he founded Chariot Innovations Inc., to bring the technology to market. His specific projects have included the study of human, horse, and camel gait motion characteristics, the study of on-body electromagnetic wave transmission characteristics, and computer modeling methods and algorithms to represent human arm biomechanics, to process and characterize periodic motion patterns, and to analyze anatomical features in medical images. He has served as a PI and a Co-PI for a variety of grant projects funded through state and local agencies, including NSF. One funded multi-disciplinary project studies the therapeutic effects in children with autism of a treatment program involving MiraColt. He holds multiple patents for the design of various exercise and therapy devices, and for computer algorithms. His research interests include mechanical system design with computer modeling and simulation toward applications in biomechanics.

YANG LI (Senior Member, IEEE) received the B.S. degree in electrical engineering from the University of Science and Technology of China, in 2005, and the M.S. and Ph.D. degrees in electrical and computer engineering from The University of Texas at Austin, in 2007 and 2011, respectively.

He joined as a Faculty Member with Baylor University, in 2011, where he is currently an Associate Professor of electrical and computer engineering. He has authored 38 journal articles and 67 conference papers and abstracts. His research interests include body area electromagnetic wave propagation and antenna radiation, wearable antenna analysis and design, effective medium theory and homogenization technique, and micro-doppler radar. He serves as the General Co-Chair for the 2022 IEEE Texas Symposium on Wireless and Microwave Circuits and Systems.